INFINITE BEAMFORMING: WAVENUMBER DECOMPOSITION OF SURFACE PRESSURE FLUCTUATIONS

Stefan Haxter[1] and Carsten Spehr[1]
[1]Deutsches Zentrum für Luft- und Raumfahrt (DLR)
German Aerospace Center
Bunsenstr. 10, 37073 Göttingen, Germany

ABSTRACT

The fluctuating pressure field underneath a turbulent boundary layer can lead to excitation of the surface structure of airplanes, trains and cars. At high flow speeds, this excitation becomes a major noise source in the vehicle interior. In the past, the characteristics of this excitation have been measured by the DLR in wind tunnels and in flight tests. A beam forming technique using planar waves was used as wavenumber decomposition in order to analyze the pressure fluctuations present over an installed microphone array. The information contained in the wavenumber spectrum resulting from the analysis is essential when empirically modeling the excitation behavior of a surface exposed to a pressure field. Speed, direction, and propagation mechanism (acoustic or hydrodynamic) of pressure waves can be determined from the position of sources in the wavenumber domain. This makes the wavenumber decomposition a helpful tool for the characterization of source mechanisms. In this paper, a summary of the test results is given. The attributes and potential of the wavenumber decomposition are emphasized in particular.

1 INTRODUCTION

The excitation of surface structures exposed to fields of fluctuating pressure is known to be a major source mechanism for vehicle interior noise. Although the representation of the characteristics of this fluctuating pressure in the wavenumber domain has been known for decades [1], the measurement of this representation had not been conducted for a long time. In 2002 Bremner proposed the combined consideration of aero-vibro-acoustics and identified its importance in vehicle design [2]. Arguillat et al. [3] measured the wavenumber spectrum using a rotary array in 2005, while in 2008 Ehrenfried & Koop [4] used high speed wind-tunnel measurements to demonstrate that it is possible to distinguish between acoustical pressure fluctuations and hydrodynamic pressure fluctuations by location in the wavenumber domain. The latter also used the location of the acoustic waves to distinguish between wind tunnel noise and desired acoustic waves emitted from the measurement object [5]. Haxter &

Spehr [6] used flight test data to investigate the characteristics of hydrodynamic and acoustic pressure fluctuations in a real flight scenario. Recent publications [7, 8] have shown that wavenumber decomposition is becoming increasingly popular in an industrial context. Therefore, in this paper, a brief overview of the advantages, limitations, potentials, and characteristics of the wavenumber decomposition will be given.

2   DATA PROCESSING

2.1   Wavenumber Decomposition

In standard beam forming, the amplitude and phase information of the pressure field signals measured at different positions in an array are evaluated by application of a monopole source model. For wavenumber decomposition, the source model is exchanged by a planar wave model. The desired parameter which makes up the steering grid is no longer the source position but rather the wavenumber and direction of the waves propagating over the array. The wavenumber decomposition can be seen as a Fourier transformation of the pressure fluctuations from the spatial domain into the wavenumber domain. In the following, b denotes the beamforming output and R is the cross-correlation matrix. ξ and η are the distances between each transducer combination.

$$b(k_x, k_y, \omega) = \frac{1}{(2\pi)^2} \int_{-\infty}^{+\infty}\int_{-\infty}^{+\infty} R(\xi, \eta, \omega) \cdot e^{-2\pi i (k_x \xi + k_y \eta)} d\xi \, d\eta \tag{1}$$

The transformation is conducted for each frequency ω as a beam forming algorithm using uniform beam former. N is the number of transducer combinations used for correlation.

$$b(k_x, k_y, \omega) = \frac{\tilde{e}^H \underline{\underline{R}}(\omega) \tilde{e}}{N} \tag{2}$$

A planar wave model is used for the propagation of the pressure fluctuations. $\tilde{e}$ is called the steering vector.

$$\tilde{e} = \exp(-2\pi i \cdot (k_x \underline{x} + k_y \underline{y})) \tag{3}$$

The steering grid contains all the wavenumbers k_x and k_y chosen for correlation. The wavenumber in this notation has units of cycles per metre (as opposed to the usual units of angular wavenumber). Each steering vector $\tilde{e}$ contains information about the modelled phase information at all sensor locations $\underline{(x, y)}$.

A wavenumber decomposition results in the wavenumber spectrum $b(k_x, k_y, \omega)$. The spectrum – or parts of it – can be transformed back from the wavenumber domain to the spatial domain. This is given by equation (4), where A denotes the integration area of interest. The mean power spectrum of all the transducers is obtained at $R(0,0,\omega)$. In equation (4), $q(k_x, k_y, \omega)$ is the source map retrieved by application of a deconvolution procedure described in references [4] and [9].

$$R(\xi, \eta, \omega) = \iint_A q(k_x, k_y, \omega) \cdot e^{2\pi i (k_x \xi + k_y \eta)} dk_x dk_y \tag{4}$$

2.2   Distinction between acoustic and hydrodynamic pressure fluctuations

Different positions in the wavenumber domain are related to different wave propagation speeds and directions. By means of speed, discrimination between different wave characteristics is possible. Pressure fluctuations located on the border of and within the so-called acoustic domain are of acoustic nature, whereas those located outside this domain are of hydrodynamic nature. A main cause of hydrodynamic pressure fluctuations is turbulent pressure fluctuations being transported by convection in a boundary layer over a surface. The acoustic domain is given by: (ref. [4, 5])

$$\frac{k_x}{k_o} = \frac{\cos\theta}{1 + M\cos\theta} \quad \text{and} \quad \frac{k_y}{k_o} = \frac{\sin\theta}{1 + M\cos\theta} \tag{5}$$

In equation (5), k_0 denotes the wavenumber of waves propagating at the speed of sound at the evaluation frequency. It is also called the "acoustic wavenumber". θ denotes the angle from the center of the wavenumber spectrum at $k_x = 0$ and $k_y = 0$. All waves that appear on the rim of the acoustical domain propagate at the speed of sound. These waves have no inclination towards the array plane and the position on the perimeter of the domain represents the wave propagation direction. In figure 1, all waves wave appearing at $k_x > 0$ propagate in positive x-direction (from left to right) and all waves appearing at $k_x < 0$ propagate in negative x-direction (from right to left). The same applies for the k_y-direction.
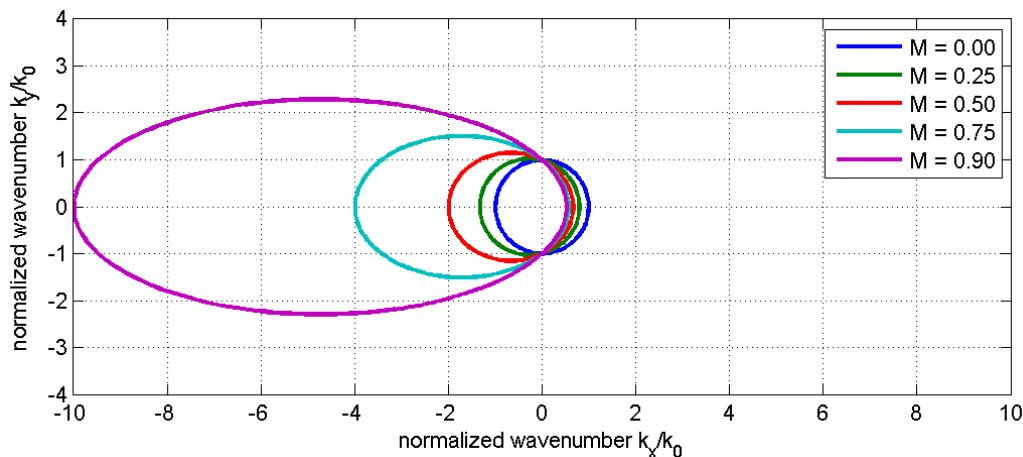
Fig. 1: Variation of the acoustic domain with different Mach numbers

The boundary of the acoustic domain is Mach-number-dependent: As the Mach number is increased, the acoustic domain is stretched towards the direction from which the flow comes. In figure 1, the flow is in the positive x-direction, so that the acoustic domain is stretched towards negative k_x-values. All the waves propagating upstream are constantly convected downstream with the flow. The resulting pressure field on the surface is therefore compressed in the upstream direction and expanded in the downstream direction.

If the angle of incidence perpendicular to the array is increased, the position of this wave will shift towards the center of the acoustic domain. The reason for this is the increased wavelength on the surface displayed in figure 2. Since the frequency of the wave is constant,

the increased wavelength measured results in an increased phase velocity of the pressure fluctuations on the surface.
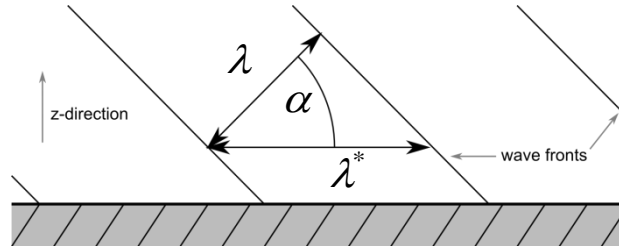
Fig. 2: Increase of wavelength on the surface with incident angle

As mentioned before, all waves that appear outside the acoustic domain are not of acoustic but rather of hydrodynamic nature. An important source of hydrodynamic pressure fluctuations on the surface of a structure is when this structure lies underneath an unsteady flow field. Here, a turbulent boundary layer on the surface contains vortex structures which are convected downstream, leaving a distinct "pressure fluctuation footprint" on the surface. As they propagate downstream, the vortex structures alter due to the viscosity of the fluid and dissipation. Therefore, these hydrodynamic pressure fluctuations have a pronounced spatial decorrelation in contrast to acoustic pressure fluctuations. They do not extend as far as the acoustic pressure fluctuations and as a result, convective sources appear as a broadband "convective ridge" rather than a point source in the wavenumber domain. The center of the convective ridge is at the convective wavenumber and contains information about the convection velocity of turbulent structures in the boundary layer. The amplitude of the convective velocity is given by

$$|u_c| = \frac{f}{|k_c|} \tag{6}$$

where f is the current evaluation frequency and $|k_c|$ is the distance of the origin of the spectrum to the center of the convective ridge in [1/m]. The direction of convective propagation of the turbulent structures is given by

$$\alpha_c = \arctan\frac{k_{c,y}}{k_{c,x}} \tag{7}$$

with the position of the center of the convective ridge given by $k_{c,x}$ and $k_{c,y}$.

2.3 Array Pattern

The pressure fluctuations on a surface are measured with an array. When evaluating the data, the characteristics of the array transducer distribution are imposed on the results. This characteristic is called the array pattern. It describes how a single source is evaluated by the array and represented in the wavenumber domain. In Figures 2 (a) and (b), two examples of two-dimensional arrays are shown. The array on the left has equidistant spacing of $\Delta k_x = \Delta k_y = 0.1\,\mathrm{m}$ between the transducers, while the array on the right has non-equidistant spacings.

The array patterns pertaining to each array are shown in figure 2 with a pressure fluctuation of wavenumber of $k_x = k_y = 0$ acting upon it. The patterns of both arrays have their main lobe in the center of the map at $k_x = k_y = 0$. However, for the pattern of the equidistant array on the left, side lobes identical to the main lobe appear at multiples of 10m^{-1}. This is caused by aliasing, as the identical side lobes appear at the inverse of the minimum spacing in between two transducers.

The array pattern of the non-equidistant array shown on the right has side lobes as well. Although being more numerous in the wavenumber area under consideration, all these side lobes have amplitudes 10dB below that of the main lobe. The non-equidistant spacing of the transducers makes aliasing effects appear at considerably greater wavenumbers than in the equidistant case. The reason for this is that identical side lobes appear at wave numbers that are the reciprocal of the greatest common divisor of the distances in between the positions. It does not depend on the minimum spacing.
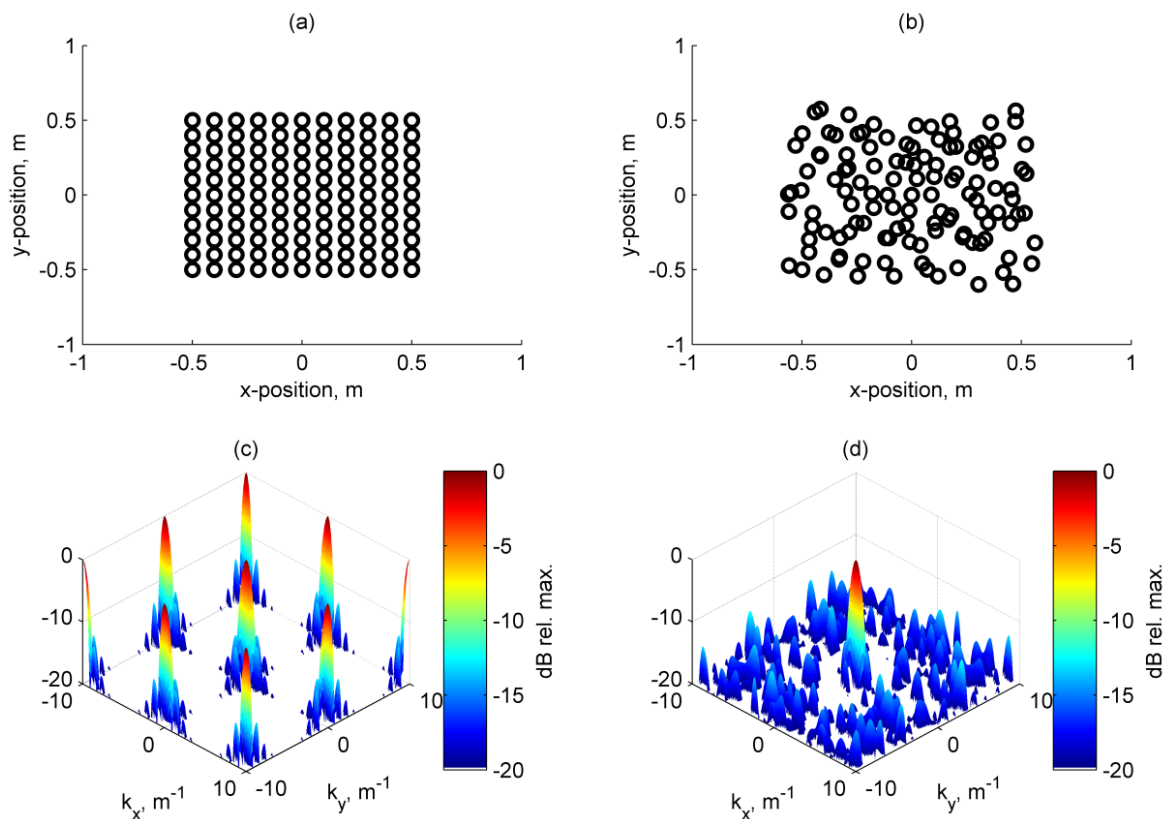
Fig. 2: *(a) equidistant transducer distribution; (c) corresponding array pattern.*
(b) quasi-random transducer distribution; (d) corresponding array pattern

3   EXPERIMENTAL SETUP

Two experimental setups will be shown for a demonstration of the capability of wavenumber decomposition.

The first setup is a wind tunnel experiment at a high subsonic speed of $M = 0.6$. Forty-eight pressure transducers were used in an array to measure the pressure fluctuations underneath a turbulent boundary layer. The array was mounted into a flat plate with a run

length of approximately 2.5m upstream of the array for the boundary layer to develop. A detailed test setup is given in reference [4].

Table 1: Measurement conditions

	Wind tunnel	Flight test
u_{Array} [m/s]	210.4	212.0
M_{Array}	0.6	0.69
T_{∞} [°C]	≈ 35	-36
f_s [kHz]	120	50
n_{FFT}	2^{13}	2^{12}
Δf [Hz]	14.65	12.20
δ [m]	≈ 0.03	≈ 0.15
Re_{δ}	$1.89 \cdot 10^5$	$1.17 \cdot 10^6$

4   RESULTS

In figure 3, a wavenumber spectrum from the flight test is shown at a frequency of 1502Hz. A distinct peak is visible within the acoustic domain: the blade passing frequency of the engine fan. The peak is very sharp and this is an indication for a spatially highly coherent signal present over the array. The amplitude of the peak is very high. Information about the convective transport of turbulent structures in the boundary layer is completely covered by the side lobes of the array pattern.

However, at the higher frequency of 1630 Hz the convective ridge is clearly visible as the dominant feature in the wavenumber spectrum in figure 4, and. no acoustic peaks can be seen. They are either not present, or covered by the dominant convective ridge. The flow direction can be tracked as the vector from the center of the spectrum to the center of the convective ridge.
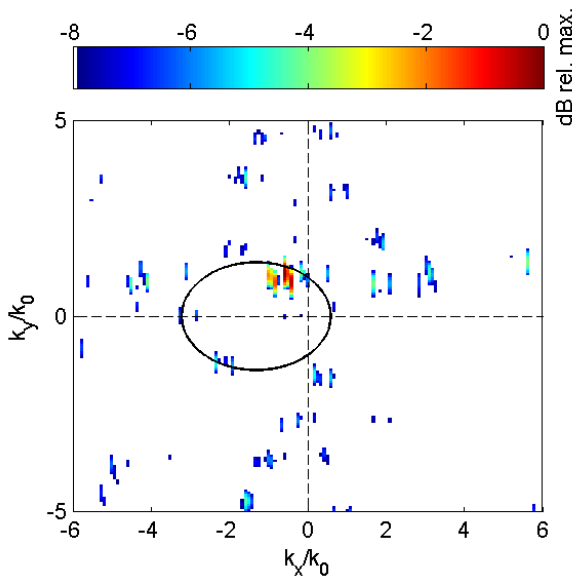
Fig. 3: *Wavenumber spectrum from the flight test at f=1502Hz (from ref. [11])*
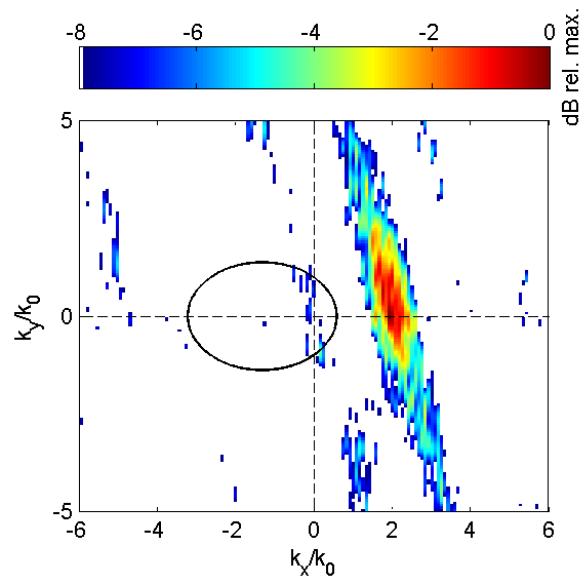
Fig. 4: *Wavenumber spectrum from the flight test at f=1630Hz (from ref. [11])*
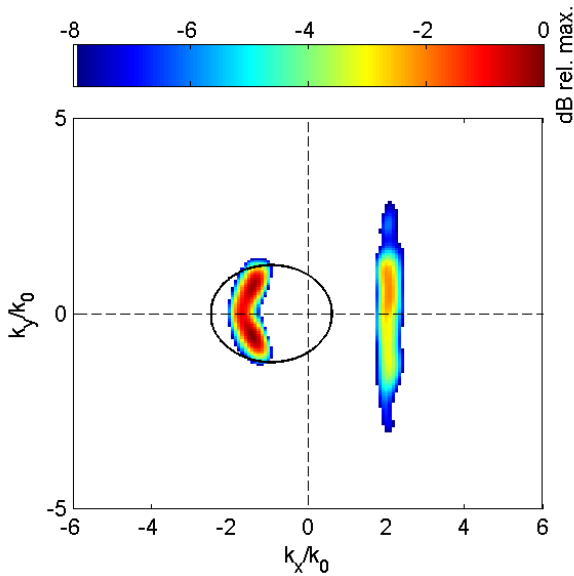
Fig. 5: Wavenumber spectrum from the wind tunnel test at f=1480Hz
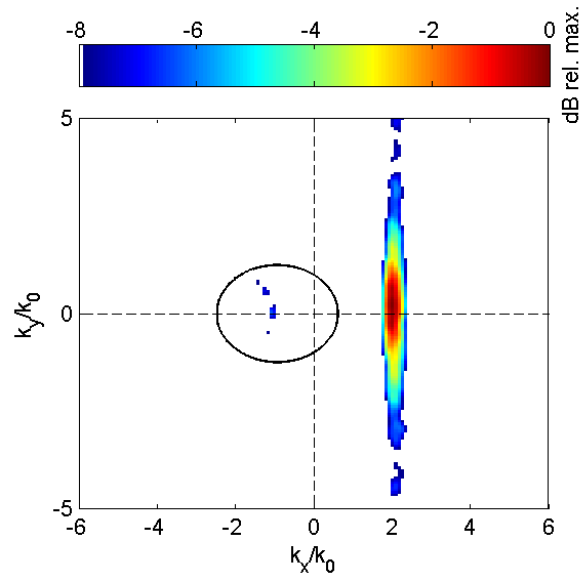
Fig. 6: Wavenumber spectrum from the wind tunnel test at f=2454Hz

In the case under consideration, the flow is diverted approximately 13° upwards. The orientation of the convective ridge is also tilted and remains perpendicular to a line from its center to the origin of the spectrum. The elongation of the convective ridge gives an indication of the extent of the spatial decay of turbulent structures in the boundary layer. A description and detection of this parameter in the spacing domain can be found in reference [12]. It can be compared to the wind tunnel measurements.

The same evaluation as for the flight test was applied to the wind tunnel data. In figure 5, a wave number spectrum from the wind tunnel test is shown for f = 1480 Hz. Two acoustic waves can be seen to propagate upstream: one has a tendency towards negative k_y-direction and the other has a symmetrical tendency towards positive k_y-direction. Their actual position in the acoustic domain is not on the rim but within the domain: the waves strike the array at an inclined angle. A convective ridge is visible in the right half of the spectrum. The amplitude of the spectrum in the acoustic domain is higher than outside.

In figure 6, an evaluation from the same test at a frequency of 2454Hz is shown. Very little acoustic energy is visible; the convective ridge is the dominant feature at this frequency. Flow direction is again from the origin of the spectrum towards the center of the convective ridge. The convective ridge appears more slender here than in the flight test case. From a signal processing point of view, this results from a coherent pressure signal being present over a longer distance than in the flight test case. This indicates a longer distance travelled by the turbulent structures before losing their identity.

In figures 7 and 8, the separate integrals of the acoustic and hydrodynamic spectra are shown along with a directly determined mean power spectrum of all transducers. In the wind tunnel case in figure 7, the pressure fluctuation levels are higher than in the flight test case in figure 8.

In the wind tunnel very high levels of acoustic pressure fluctuation are present at frequencies below 1500Hz. These acoustic pressure fluctuations are caused by the noise in
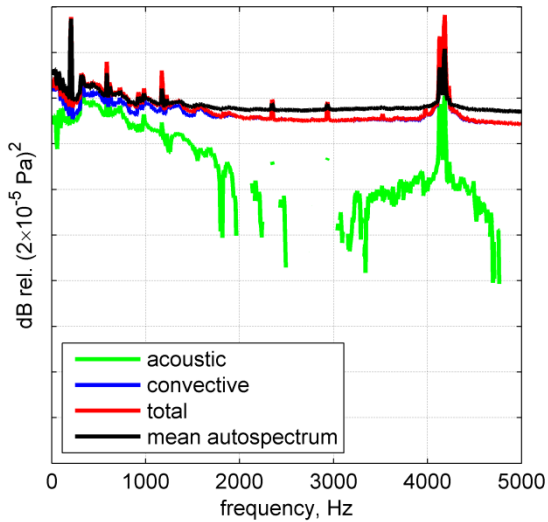
Fig. 7: Separately integrated spectra from the wind tunnel test (from ref. [11])
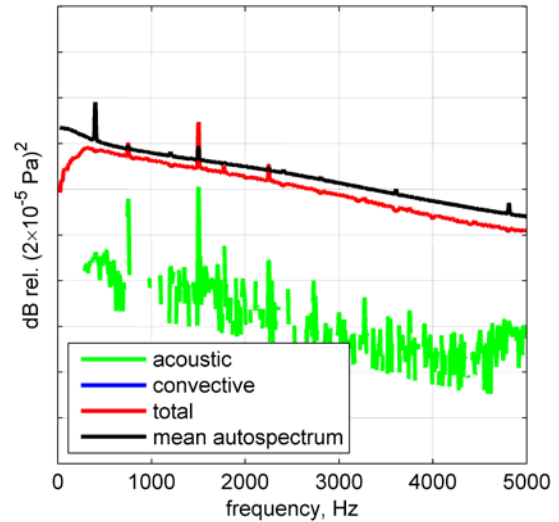
Fig. 8: Separately integrated spectra from the flight test (from ref. [11])

the closed test section. Above 1500Hz, the hydrodynamic pressure fluctuations are the dominant feature, except at a frequency of approximately 4000Hz. Here, most probably, a channel mode is present.

In the flight test, the acoustic pressure fluctuations are considerably lower than the hydrodynamic pressure fluctuations, except at the blade passing frequency. At 1500Hz and one-half that frequency, a sharp rise in the acoustical energy is visible.

The hydrodynamic pressure fluctuations in the flight test become attenuated at higher frequencies. This is not the case for the pressure fluctuations in the wind tunnel in the frequency range under consideration.

The convective velocity resulting from the distance of the center of the convective ridge to the origin of the spectrum is plotted in figure 9 for both the flight test and the wind tunnel experiment. Although the boundary layer in the flight test is considerably thicker than in the wind tunnel experiment, the convective transport of the turbulent structures appears similar.

Below a frequency of 1500Hz, the convective ridge was not seen underneath the dominant acoustic sources, so that its determination could not be carried out.
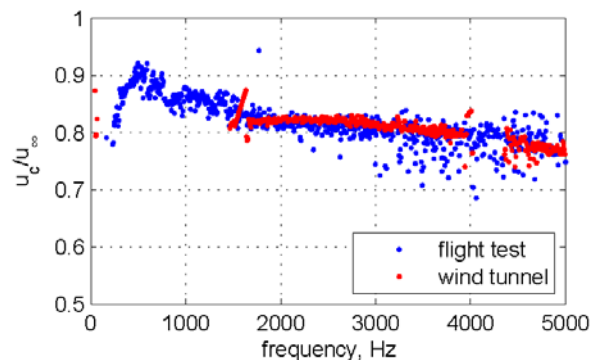
Fig. 9: Convective speed in the turbulent boundary layer of the pressure fluctuations in the flight test and in the wind tunnel (from ref. [11])

5   SUMMARY

Wavenumber decomposition was applied to data from a transducer array underneath a turbulent boundary layer in both a wind tunnel and a flight test experiment. Information about the pressure fluctuations over the array was obtained from the resulting wavenumber spectra: amplitude of acoustically and hydrodynamically caused pressure fluctuations, the direction and inclination of acoustic waves striking the array, the speed and direction of the convection of hydrodynamic pressure fluctuations and a brief comparison of the distances over which the turbulent structures in the boundary layer keep their identity.

The information presented here has been deduced solely from a single diagram resulting from wavenumber decomposition. When examining the capability of pressure fluctuations exciting a structure underneath a flow, the wavenumber decomposition method provides a valuable tool for the identification of the sources involved.

REFERENCES

[1]   M. K. Bull. "Wall-Pressure Fluctuations Beneath Turbulent Boundary Layers: Some Reflections on Forty Years of Research" J. Sound Vib, 190, Issue 3, 1996, 299-315. Doi: 10.1006/jsvi.1996.0066

[2]   Bremner, P and Wilby, J. "Aero-Vibro-Acoustics: Problem Statement and Methods for Simulation-based Design Solution" AIAA-2002-2551, 2002. 8th AIAA/CEAS Aeroacoustics Conference, Breckenridge, CO, USA, 17-19 June 2002.

[3]   Arguillat, B., Ricot, D., Robert, G., Bailly, C. "Measurements of the Wavenumber-Frequency Spectrum of Wall Pressure Fluctuations under Turbulent Flows" AIAA-2005-2855. 11th AIAA/CEAS Aeroacoustics Conference, Monterey, CA, USA, 23-25 June 2005.

[4]   Ehrenfried, K and Koop, L. "Experimental study of pressure fluctuations beneath acompressible turbulent boundary layer" AIAA-2008-2800, 2008. 14th AIAA/CEAS Aeroacoustics Conference, Vancouver, BC, 5-7 May 2008.

[5]   L.Koop and K.Ehrenfried. "Microphone-array processing for wind-tunnel measurements with strong background noise" AIAA-2008-2907, 2008. 14th AIAA/CEAS Aeroacoustics Conference, Vancouver, BC, 5-7 May 2008.

[6]   S.Haxter and C.Spehr. "Two-Dimensional Evaluation of Turbulent Boundary Layer Pressure Fluctuations at Cruise Flight Conditions" AIAA-2012-2139, 2012. 18th AIAA/CEAS Aeroacoustics Conference, Colorado Springs, CO, USA, 4-6 June 2012.

[7]   Hartmann, M. and Ocker, J. and Lemke, T. and Mutzke, A. and Schwarz, V. and Tokuno H. and Toppinga, R. and Unterlechner, P. and Wickern, G. "Wind Noise caused by the A-pillar and the Side Mirror of a Generic Vehicle Model" AIAA-2012-2139, 2012. 18th AIAA/CEAS Aeroacoustics Conference, Colorado Springs, CO, USA, 4-6 June 2012.

[8]   Gabriel, C. and Müller, S. and Lerch, R. and Ullrich, F. "Measurement of the Spatial Coherenc of Surface Pressure in the Wake of a Car's Side Mirror" AIAA-2013-2059, 2013. 19th AIAA/CEAS Aeroacoustics Conference, Berlin, Germany, 27-29 May 2013.

[9]   Ehrenfried, K., Koop, L., 2007. "Comparison of iterative deconvolution algorithms for the mapping of acoustic sources." AIAA Journal 45, pp.1584-1595.

[10] C.Spehr et al. "In-Flight Sound Measurements: A First Overview" AIAA-2012-2207, 2012. 18th AIAA/CEAS Aeroacoustics Conference, Colorado Springs, CO, USA, 4-6 June 2012.

[11] Haxter, S. and Spehr, C. "In-Flight Determination of Acoustic and Hydrodynamic Pressure Fluctuations" In *Deutsche Jahrestagung für Akustik* (AIA-DAGA 2013), Meran, März 2013

[12] Haxter, S. and Spehr, C. "Examination of the Influence of Flow Speed on the Coherence Lengths in Turbulent Boundary Layers at High Subsonic Mach Numbers" In: *New Results in Numerical and Experimental Fluid Mechanics IX*, Springer Berlin, ISBN : 978-3-319-03157-6